



Effect of liquid viscosity on the performance of a non-porous membrane contactor for CO₂ capture

Ida M. Bernhardsen^a, Luca Ansaloni^{a,b}, Hanne K. Betten^{a,c}, Liyuan Deng^a, Hanna K. Knuutila^{a,*}

^a Department of Chemical Engineering, Norwegian University of Science and Technology (NTNU), Trondheim NO-7491, Norway

^b SINTEF Industry, Sustainable Energy Technology, Oslo, Norway[†]

^c Jotun AS, Performance Coatings, Powder Segment, Sandefjord, Norway[†]

ARTICLE INFO

Keywords:

CO₂ capture
Mass transfer coefficient
Absorbent viscosity
Non-porous membrane contactor

ABSTRACT

The effect of liquid viscosity on the performance of a non-porous membrane contactor is important to study for a proper solvent selection and process design. In this work, the overall mass transfer coefficient for MEA- and NaOH-based solutions was studied using a string of discs contactor in the temperature range 28–64 °C and a thin composite membrane contactor at 40 °C. Also, viscosity, density and N₂O solubility of the aqueous solutions were measured in the temperature range 30–70 °C. The solvent viscosity of MEA and NaOH solutions was artificially adjusted from 0.5 to 54.7 mPa s by addition of sugar and/or glycerol.

The overall mass transfer coefficient was found to decrease with increasing amount of viscosifier and the decrease seemed to be independent of the solvent system. In the membrane contactor, the decrease in the overall mass transfer coefficient was attributed to the decreasing CO₂ solubility and CO₂ diffusion coefficient, but as these properties alone were not able to describe the experimental values, the reason was attributed also to the establishment of an additional resistance at the membrane/liquid interface.

1. Introduction

The Paris agreement sets a goal to limit the global temperature rise to well below 2 °C. However, two years after it went into force, the emissions are heading in the opposite direction to the cuts needed to combat climate change. According to a report by the Global Carbon Project, carbon emissions from coal, oil, natural gas and cement production are expected to increase by 2.7% in 2018 compared to the previous year [1]. Thus, in response to increasing emissions, several climate actions need to be implemented. For instance, an increase in the use of renewable energy (hydropower, wind, solar), the creation of energy efficient solutions and implementation of carbon capture and storage (CCS) represent concrete perspectives. CCS is a promising solution to decarbonize the energy and industrial sectors as it can capture up to 90% of produced CO₂ from large emission sources such as coal-fired power plants and cement, iron and steel production plants [2], thereby preventing CO₂ from entering the atmosphere. After the CO₂ is captured, it is transported and stored safely and permanently in geological formations.

Today, several CO₂ capture technologies exist. Among the technologies available for post-combustion CO₂ capture, chemical absorption

using aqueous amine solvents has the highest technology readiness level (TRL) with a TRL of 9 [3]. In a typical chemical absorption process, CO₂ is brought in direct contact with the solvent in packed columns and absorbed into the solvent at around 40 °C. Upon heating at around 120 °C, the CO₂ is released from the solution. The technology can be retrofitted to already existing plants and has been proven in two commercial-scale facilities from coal-fired power plants, Boundary Dam in Saskatchewan, Canada, and Petro Nova in Texas, USA. However, despite technical maturity, the research efforts are still focused on making the technology economical viable and improving the solvent performance, which implies finding solvents with improved energy requirement, absorption rate and cyclic capacity, which are thermally stable at process conditions [4–7]. Another concern is the environmental impact of large scale use of amines as the emission of degraded solvents to the environment may occur through the exhaust gas [8]. Therefore, to mitigate this issue a promising alternative to the conventional absorption column is the use of non-porous membranes in membrane contactors [9]. The membrane is the interface between the gas and liquid phase and, by materials engineering, can be designed to act as barrier for target components (i.e., amine), while still allowing high CO₂ fluxes towards the liquid absorbent. Ansaloni et al. [10]

* Corresponding author.

E-mail address: hanna.knuutila@ntnu.no (H.K. Knuutila).

[†] Present address.

Nomenclature

c	concentration, mol/m ³
D _{CO₂} ^g	diffusivity of CO ₂ in the gas phase, m ² /s
E	enhancement factor
H	Henry's law constant, (kPa m ³)/mol
k _{dl}	mass transfer coefficient associated with the dense layer, m/s
k _g	gas-side mass transfer coefficient, mol/m ² kPa s
k _l	liquid-side mass transfer coefficient, m/s
k _l ⁰	liquid-side mass transfer coefficient without reaction, m/s
k _m	mass transfer coefficient of the membrane, m/s
K _{ov}	overall mass transfer coefficient, m/s
k _{ps}	mass transfer coefficient of the porous support, m/s
N	absorption flux, mol/m ² s
p	pressure, kPa
P	permeability, m ³ (STP)/(m s Pa)
R	universal gas constant, m ³ Pa/(K mol)
T	temperature, K
v _m	molar volume, m ³ /mol

y mole fraction

Greek symbols

δ	thickness of the different membrane layers, m
ε	porosity of the porous support
μ	viscosity, mPa s
τ	pore tortuosity

Abbreviations

AARD	average absolute relative deviation
MC	membrane contactor
MEA	monoethanolamine
NaOH	sodium hydroxide
LM	logarithmic mean
SDC	string of discs contactor
TCM	thin composite membrane
TIC	total inorganic carbon

reported that fluorinated polymers are characterized by a high CO₂/amine transport selectivity, and their use as membrane material can considerably reduce the amine concentration in the gas phase leaving the absorber [11]. Furthermore, the use of thin composite membranes (porous support coated with a thin dense layer) is beneficial to prevent the membrane wetting in the membrane contactor. Compared to a traditional absorption column, a higher mass transfer resistance is expected due to the presence of a membrane, even though the opposite has also been reported [12,13].

In a recent study, the CO₂ capture performance of blended amines was studied using a non-porous membrane contactor [14]. The study found that the mass transfer coefficient at room temperature for the blended amines was 50% lower than the benchmark 30 wt% monoethanolamine (MEA). As the difference in mass transfer decreased with increasing temperature, the higher solvent viscosity of the blended amines was suggested as a potential reason to explain the lower mass transfer coefficient. However, along with the viscosity drop, the increase of the operating temperature also affected other properties (i.e., decrease of transmembrane CO₂ flux, higher CO₂ diffusion in the interface (liquid/membrane) layer and lower CO₂ absorption capacity of the liquid). Therefore, even though viscosity was identified as the prime suspect, it was not possible to decouple its effects from the other.

A good understanding and prediction of the mass transfer in viscous solutions is important for proper solvent selection and process design. Amine solvents can typically have 5–10 times higher viscosities than water and viscous solutions decrease the diffusion of CO₂ into the solvent. Upon CO₂ loading, these differences can become even larger [14]. In literature, the influence of viscosity on the liquid mass transfer coefficient without reaction, k_l⁰, has been studied in packed columns, but not yet in membrane contactors. In packed columns, the k_l⁰ is found to decrease with increasing solvent viscosity [15–18]. Traditionally, sugar and glycerol have been used to increase the solvent viscosity due to their complete solubility in water and Newtonian behavior [18–21].

Song and Rochelle [21] studied the reaction kinetics of CO₂ in aqueous solutions of sodium hydroxide (NaOH) and glycerol using a wetted wall column (WWC). The study showed that the CO₂ absorption rate increased with the addition of 15 wt% glycerol to NaOH and decreased with the addition of 20–80 wt% glycerol to NaOH. The increase in absorption rate was likely due to the formation of glyceroxide, while the decrease was likely due to decreasing diffusivity of CO₂.

In this work, the effect of liquid viscosity on the membrane performance was studied using MEA and NaOH solutions. The viscosity was artificially changed with the addition of sugar and glycerol (Fig. 1)

while keeping the concentration of MEA and NaOH constant. The overall mass transfer coefficient (K_{ov}) for the different aqueous solutions was obtained using a string of discs contactor (SDC) in the temperature range 28–64 °C, and a membrane contactor (MC) at 40 °C. In addition, viscosity, density, and N₂O solubility were measured.

2. Chemical reactions

Absorption of CO₂ into the aqueous solutions of MEA or NaOH involves several reactions. In both solutions, CO₂ dissolves into the solution and reacts with OH⁻ to form (bi)carbonate (Eqs. (1)–(3)).



In addition, in the aqueous solution of MEA, MEA reacts with CO₂ to form carbamate. The formation of carbamate can be described using two different reaction mechanisms, the zwitterion mechanism [22] and the termolecular mechanism [23]. The zwitterion mechanism is a two-step reaction mechanism in which the formation of carbamate proceeds through the formation of a zwitterion complex as given in Eqs. (4) and (5)

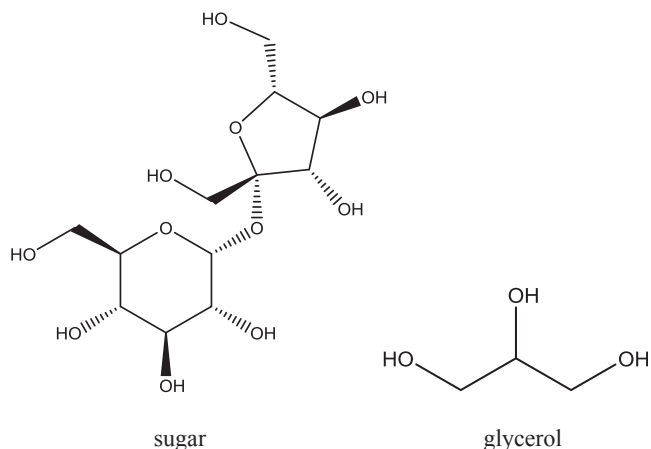
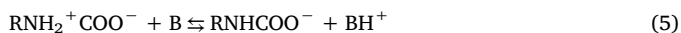
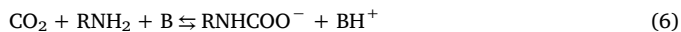


Fig. 1. Molecular structure of sugar and glycerol.

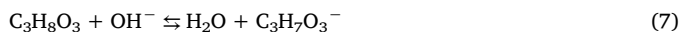


where B is any base present in the solution acting as a counter-ion (MEA or H₂O).

The termolecular mechanism suggests that the reaction between CO₂, MEA and a base occur in a single-step through a loosely-bound encounter complex as the intermediate (Eq. (6)).



In addition, literature report that in a basic solution glycerol can react with OH⁻ to form glyceroxide (Eq. (7)) [24], which again can react with CO₂ (Eq. (8)) [25]. These reactions may also be applicable for sugar, which, similar to glycerol, contains several hydroxyl groups (Fig. 1).



3. Experimental

3.1. Materials

Monoethanolamine (CAS: 141-43-5) with purity ≥ 98% and glycerol (CAS: 56-81-5) with purity ≥ 99.5% were purchased from Sigma-Aldrich, sodium hydroxide (CAS: 1310-73-2) with purity 99.1% was purchased from VWR chemicals and sugar was of a commercially-available grade. Nitrogen oxide (CAS: 10024-97-2) with purity 99.999%, carbon dioxide (CAS: 1244-38-9) with purity 99.999% and nitrogen (CAS: 7727-37-9) with purity 99.998% were purchased from AGA. Teflon AF2400 (CAS: 37626-13-4) was purchased from Chemours Company. FC-72 (CAS: 86508-42-1) was supplied by 3 M. Celgard LLC (Charlotte, US) kindly supplied the porous polypropylene (PP) support (Celgard® 2400, thickness 25 μm, porosity 41%). All chemicals were used as received without further purification. The aqueous solutions studied were 30 wt% MEA mixed with 0, 28, 35 and 38 wt% sugar, and 3.9 wt% NaOH mixed with 0, 38, 48 and 52 wt% sugar and 50 wt% glycerol. The solutions were prepared gravimetrically with deionized water.

3.2. Methods

3.2.1. pH measurement

The pH value of aqueous solutions was measured at 25 °C using an InLab NMR pH electrode connected to a SevenEasy pH meter from Mettler Toledo. Before the measurement, the pH electrode was calibrated at pH 7.00, 9.21 and 11.00 using technical buffer solutions from Mettler Toledo. Based on repeated measurements, the repeatability of the pH measurement was ± 0.1.

3.2.2. Viscosity and density

Viscosity and density of the MEA- and NaOH-based solutions were measured in a combined system consisting of an Anton Paar DMA 4500 density meter [26] and an Anton Paar Lovis 2000 ME rolling-ball viscometer. The measurements were conducted in the temperature range 25–70 °C. Based on repeated measurements, the repeatability of the viscosity measurements was on average 3.8%, and the repeatability of the density measurements was ± 3·10⁻³ g/cm³.

3.2.3. N₂O solubility

The solubility of N₂O into aqueous solutions was measured using the same apparatus as detailed explained in Gondal et al. [27]. The apparatus consisted of a 1L glass reactor and a gas holding vessel, pressure transmitter PCE-28 (measuring range 0–6 bar and accuracy 0.1% of full scale) and Pt100 thermocouples (± 0.1 °C). In each experiment, the reactor was evacuated both before and after the addition of around

500 g of solution. The experiments were conducted in the temperature range 30–70 °C and at each temperature the system was left to equilibrate. At the highest temperature, N₂O was added from the gas holding vessel to the reactor and equilibrium was once again established. Thereafter, the temperature was decreased, and the equilibrium was established at each temperature.

The equilibrium partial pressure of N₂O, p_{N₂O}, was determined from measured total pressures, and the amount of N₂O added from the gas holding vessel and present in the gas phase of the reactor was calculated using the Peng-Robinson Equation of state [28]. Then, from the experimental data, the Henry's law constant was calculated as given in Eq. (9)

$$H_{\text{N}_2\text{O}} = \frac{p_{\text{N}_2\text{O}}}{c_{\text{N}_2\text{O}}} \quad (9)$$

where c_{N₂O} is the concentration of N₂O in the liquid phase. The solubility of N₂O, at a given temperature, is then the inverse of Henry's law constant, multiplied by the partial pressure of N₂O above the solution.

The solubility apparatus was validated by measuring the solubility of N₂O in water. As shown in Fig. 2, the average absolute relative deviation (AARD) was 2.0% from the correlation provided by Penttilä et al. [29], and the repeatability was on average 1.3%.

3.2.4. String of discs contactor (SDC)

The CO₂ absorption rate into unloaded MEA- and NaOH-based solutions was measured using a string of discs contactor (SDC) (Fig. 3). The apparatus, previously explained by Ma'mun et al. [30], is designed for atmospheric pressure. It consists of 43 discs with a total column height of 64.5 cm and a mass transfer area of 0.0219 m². The experiments were conducted in the temperature range of 28–64 °C and at low CO₂ partial pressures (~0.2–0.3 kPa in the feed gas).

For each experiment, a CO₂ unloaded solution was placed in a 5 L glass container and pumped through the system with a constant liquid rate of around 60 ml/min. Simultaneously, a gas stream containing N₂ and CO₂ circulated the system counter-current to the falling liquid solution. The inlet gas composition was set by mass flow controllers and an IR analyzer determined the outlet CO₂ gas concentration. The IR analyzer was calibrated with mixtures of CO₂ and N₂ before and after the experiment, and both calibrations were used to determine the CO₂ concentration in the gas stream. A DP cell provided by Druck measured the pressure. The experiment was terminated when stable gas/liquid temperatures and gas composition were maintained for at least 5 mins.

After each experimental point, a liquid sample was collected for CO₂

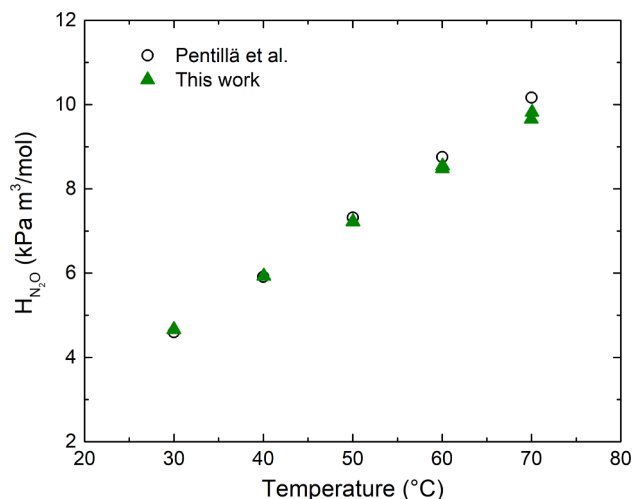


Fig. 2. Henry's law constant for N₂O in water. Literature data are obtained from Penttilä et al. [29].

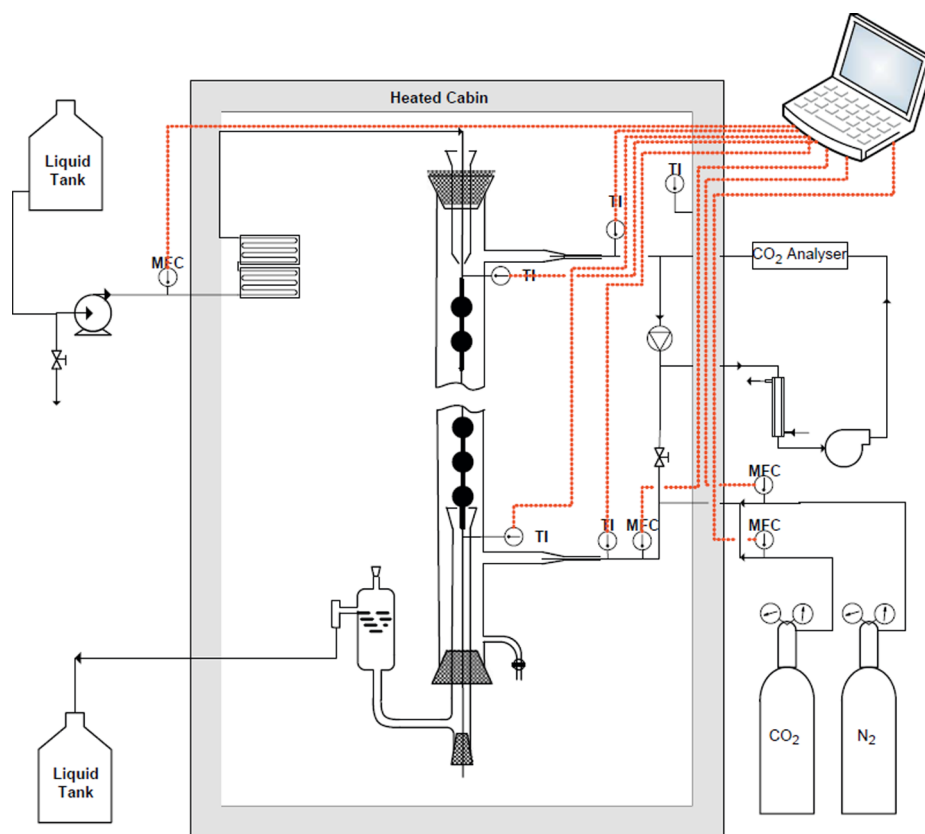


Fig. 3. Experimental set-up of the string of discs contactor. The figure is retrieved from reference [31].

and total alkalinity analysis. The final CO₂ loadings were found to be in a negligible amount (varied from 0.002 to 0.041 mol CO₂/mol alkalinity).

From the recorded experimental data, the CO₂ absorption flux and the overall mass transfer coefficient (K_{ov}) were calculated. The CO₂ absorption flux was calculated by a mass balance over the entire system (Eqs. (10) and (11)). The inlet CO₂ flux, $N_{CO_2,in}$, was measured directly by the mass flow controller, and the outlet CO₂ flux, $N_{CO_2,out}$, was calculated as given in Eq. (11) in which y_{CO_2} is the CO₂ concentration of the outlet gas phase recorded by the IR analyzer and N_{N_2} is the constant flow of inert through the apparatus.

$$N_{CO_2} = N_{CO_2,in} - N_{CO_2,out} \quad (10)$$

$$N_{CO_2,out} = N_{N_2,out} \frac{y_{CO_2,out}}{1 - y_{CO_2,out}} \quad \text{where } N_{N_2,out} = N_{N_2,in} \quad (11)$$

K_{ov} was calculated as the ratio between the absorption flux and the driving force (Eq. (12)). The driving force was calculated as the logarithmic mean of the CO₂ partial pressure difference between the outlet and the inlet stream, $\Delta p_{CO_2}^{LM}$ (Eq. (13)).

$$K_{OV} = \frac{N_{CO_2}}{\Delta p_{CO_2}^{LM}} \quad (12)$$

$$\Delta p_{CO_2}^{LM} = \frac{P_{CO_2,in} - P_{CO_2,out}}{\ln\left(\frac{P_{CO_2,in}}{P_{CO_2,out}}\right)} \quad (13)$$

To validate the experimental procedure, initial CO₂ absorption rates in 30 wt% MEA and 3.9 wt% NaOH solutions were measured and compared to literature data (Fig. 4). The calculated K_{ov} for 30 wt% MEA deviated on average 9.1% from data reported by Luo et al. [32], and the K_{ov} for 3.9 wt% NaOH agreed well with data from Gondal et al. [33]. All experiments (except for the solutions 30 wt% MEA + 38 wt% sugar and 3.9 wt% NaOH + 50 wt% glycerol) were repeated twice, and the

repeatability was on average 3.6%.

3.2.5. Liquid analysis

The CO₂ concentration in the liquid samples was determined by Total Inorganic Carbon (TIC) analysis using TOC-L provided by Shimadzu. A diluted liquid sample was injected and acidified in a 25 % H₃PO₄ solution, and the released CO₂ was detected by a non-dispersive infrared (NDIR) analyzer. The alkalinity of the liquid samples was analyzed by titrating a diluted liquid sample with 0.2 N H₂SO₄ [34].

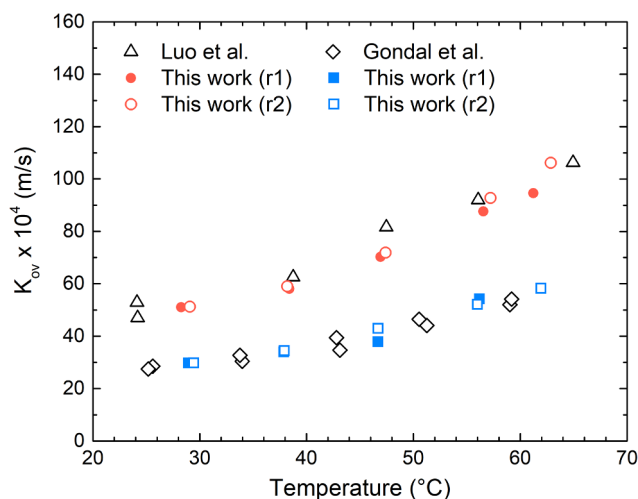


Fig. 4. Calculated values for K_{ov} as a function of temperature, for 30 wt% MEA and 3.9 wt% NaOH solutions (r1 = first run; r2 = second run). The temperature is the average of the liquid inlet and outlet temperature. Literature data are obtained from Luo et al. [32] and Gondal et al. [33].

3.2.6. Membrane fabrication and characterization

Membranes were prepared in the form of a thin composite membrane (TCM), by coating a dense layer on the top of the porous PP support. Teflon AF2400 was initially dissolved in the fluorosolvent (FC-72) in order to achieve a 1% solution on a mass base. The porous support was flattened and taped on a glass plate using aluminum tape. Subsequently, the clear polymer solution was dropped in a glass container, where the porous support was dipped twice. The second dipping happened after flipping the glass plate of 180° to ensure an even coating. Finally, the membrane was heated at 80 °C overnight to ensure the complete solvent removal (FC-72 boiling point at 1 atm = 56 °C). The final membrane morphology was analyzed using a Scanning Electron Microscope (Hitachi Tabletop TM3030) and the results are shown in Fig. 5. The surface images showed that a homogenous and defect-free coating could be achieved by means of the described coating techniques. From the cross-section image, it is possible to see that the coating thickness was in the order of $1.8 \mu\text{m} \pm 0.3 \mu\text{m}$. In addition, even though the solvent was able to wet the porous support relatively easily, no evident pore penetration was observed for the fabricated membrane. This may be related to a difference in the surface tension between the two solid materials.

In order to better understand the membrane performance in the membrane contactor tests, the surface tension of the different solutions, as well as the contact angle on the dense coating surface of the composite membrane were measured by means of an optical tensiometer (Attension Theta, Biolin Scientific). In particular, the surface tension was measured using a pendant drop technique, whereas the contact angle by means of a sessile drop method, with a liquid droplet volume of 4–6 μl and capturing images at a sampling frequency of 3 frames per second. All the tests were performed at room temperature (~ 23 °C).

3.2.7. Membrane contactor

The membrane contactor performance was investigated using the various absorbents in the rig shown in Fig. 6. The membrane is placed inside the sample holder, located inside a temperature-controlled chamber. The temperature was maintained constant at 40 °C. The gaseous stream is initially created by mixing CO₂ and N₂ coming from mass flow controllers, bypassing the cell and measuring the CO₂ content with the IR analyzer. The gas flowrate was set to 250 ml/min, and different CO₂ content (13, 30 and 50 mol%) were investigated. Meanwhile, the liquid absorbent was flown on the top side of the membrane, in contact with the dense layer, at a flowrate of 100 ml/min. Since the viscosity considerably affects the ability of the pump to provide a given flowrate, the pumping speed was calibrated for each liquid solution to ensure a constant liquid flow rate. To start the experiment, the gaseous stream was sent to the sample holder, monitoring the drop in the CO₂

concentration of the retentate stream. A more detailed description of the apparatus and the experimental procedure is reported in our previous publication [14]. K_{OV} was calculated as given by Eq. (12).

3.2.8. Modelling the CO₂ mass transfer

The CO₂ mass transfer in the SDC and the MC can be described by a resistance in series model given in Eqs. (14) and (15), respectively. In the SDC experiments, the K_{OV} is expressed from the film model which assumes that all resistance to mass transfer is restricted to two stagnant films near the gas-liquid interface (Eq. (14)). The component transport through the gas and liquid film is diffusional, in which the component transport in the liquid film is also accompanied by chemical reactions. At the gas-liquid interface, the equilibrium condition is given by Henry's law. The expression is given in Eq. (14) as following

$$\frac{1}{K_{OV}} = \frac{1}{k_g} + \frac{H_{CO_2}}{k_l} \quad (14)$$

where k_g is the gas side mass transfer coefficient, k_l is the liquid side mass transfer coefficient with reaction and H_{CO_2} is the Henry's law constant for CO₂ into the aqueous solution.

Extending the film theory and Eq. (14) to the membrane contactor case, the overall mass transfer coefficient can be described as the contribution of the three different phases: gas, liquid, and membrane. Therefore, Eq. (14) can be re-written as:

$$\frac{1}{K_{OV}} = \frac{1}{k_g} + \frac{H_{CO_2}}{k_l} + \frac{1}{k_m} \quad (15)$$

where k_m is the mass transfer coefficient of the membrane, calculated as:

$$\frac{1}{k_m} = \frac{1}{k_{ps}} + \frac{1}{k_{dl}} = \frac{\delta_{ps}\tau}{D_{CO_2}^g \varepsilon} + \frac{\delta_{dl} v_m}{PRT} \quad (16)$$

k_{ps} is the mass transfer coefficient of the porous support, whereas k_{dl} is the mass transfer coefficient associated with the dense layer. δ represents the thickness of the different membrane layers, τ is the pore tortuosity calculated as a function of the porosity (ε) of the porous support [35], $D_{CO_2}^g$ is the CO₂ diffusion coefficient in the gas phase, which can be calculated according to Fuller correlation [36], v_m is the molar volume, P is the CO₂ permeability of the dense layer, R is the gas constant and T is the operating temperature.

In this work, the overall mass transfer coefficient in the membrane contactor was modelled using Eq. (15). The mass transfer coefficient of the gas phase, k_g , was calculated with an empirical correlation described in our previous study [14] and, in view of similarity of the membrane used, the same study provided also the parameters needed

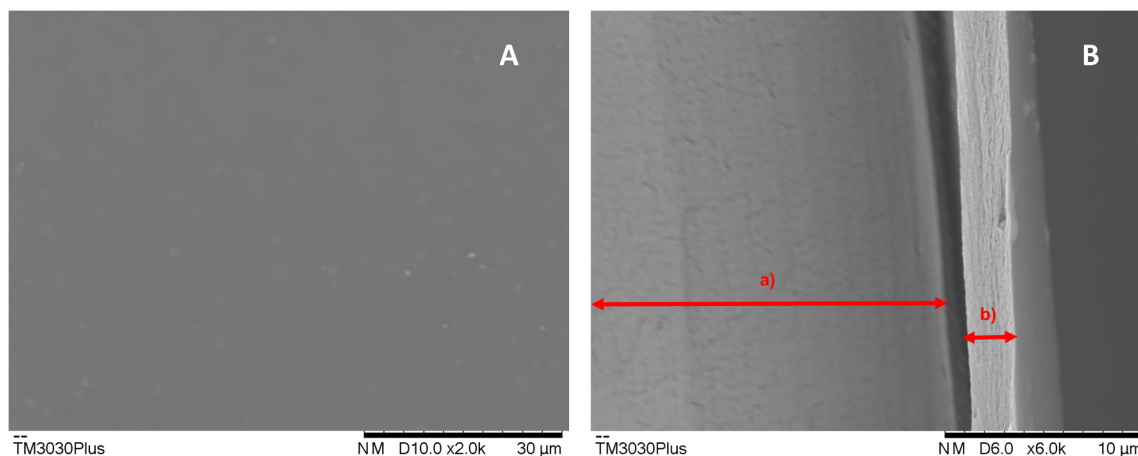


Fig. 5. Surface (A) and cross-section (B) of the TCM prepared in the present work. In the cross-section image, the letter “a” indicates the porous support, whereas the letter “b” refers to the thin dense coating.

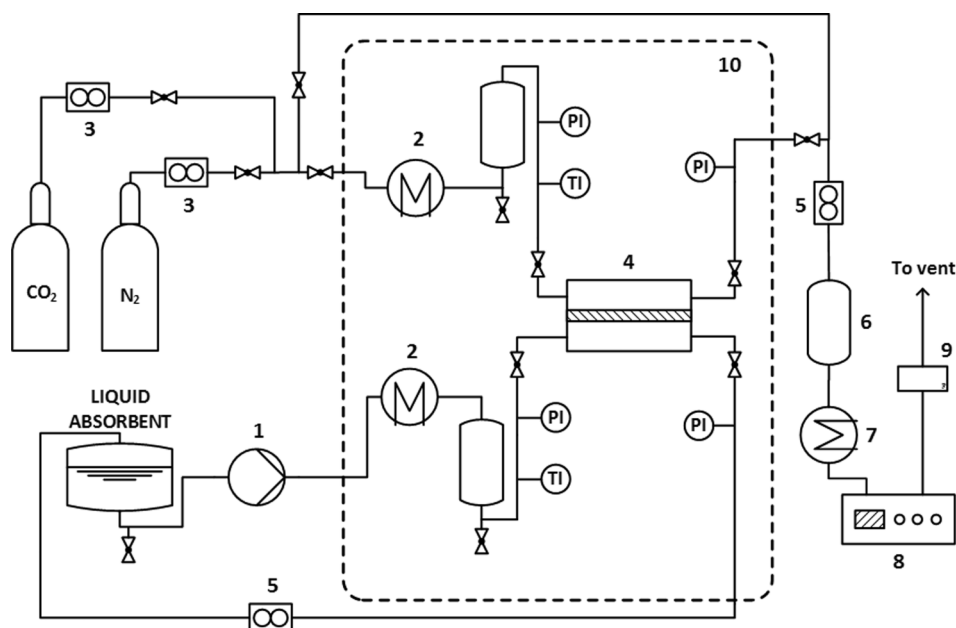


Fig. 6. Membrane contactor rig used to investigate the mass transfer coefficient (1: liquid pump; 2: heat exchanger; 3 mass flow controller; 4: membrane holder; 5: back pressure regulator; 6: acid trap; 7: condenser; 8: CO₂ IR analyzer; 9: bubble flow meter). The figure is retrieved from reference [14].

for modelling the membrane phase (Eq. (16)). Further, the Henry's law constant for CO₂ in the aqueous solutions was calculated from the N₂O-CO₂ analogy [37], where the Henry's law constant for CO₂ and N₂O in water was estimated from the correlation provided by Carroll et al. [38] and Penttilä et al. [29], respectively, and the Henry's law constant for N₂O in the aqueous solutions was experimentally determined as described in Section 3.2.3. The k_g in Eq. (14) was calculated from the correlation provided in Ma'mun et al. [30] who used the same apparatus and, by using the K_{ov} values obtained from the SDC, Eq. (14) was solved for k_l to be used in Eq. (15).

4. Results and discussion

4.1. pH at different viscosifier content

As discussed in Section 2, glycerol in aqueous solution can react with OH⁻ to form glyceroxide (Eq. (7)). Therefore, to investigate the extent to which the addition of viscosifiers (sugar or glycerol) influenced the hydrogen ion activity of the MEA- and NaOH-based solutions, the pH was measured. A change in pH value may indicate that the viscosifiers affect the reaction kinetics.

The measured pH values are listed in Table 1. From the table, it can be seen that the pH value slightly decreases with the addition of sugar and/or glycerol to the MEA and NaOH solutions. Thus, the small change may indicate that the reaction kinetics of the MEA and NaOH solutions were slightly affected by the addition of glycerol/sugar. Also, as discussed in Section 1, Song and Rochelle [21] reported an increase of CO₂ absorption rate when a small amount of glycerol was added to the caustic solution.

4.2. Liquid viscosity and density

Viscosities of MEA- and NaOH-based solutions in the temperature range 25–70 °C are presented in Fig. 7. The viscosity decreased exponentially with temperature and increased along with the amount of viscosifier. At the same temperature and with the same amount of sugar (38 wt%) added to MEA and NaOH, the viscosity increased with a factor of 15 and 8, respectively. Thus, a greater amount of sugar was added to NaOH to obtain a similar increase in viscosity as MEA. Further, the

solvent viscosities of 3.9 wt% NaOH in the blend with 38 wt% sugar and 50 wt% glycerol were similar throughout the temperature range.

Experimental density data for the MEA and NaOH-based solutions are tabulated in Table 2 and 3, respectively. The density increased with increasing concentration of the viscosifier.

4.3. N₂O solubility

The measured Henry's law constant for N₂O into MEA- and NaOH-based solutions is shown in Fig. 8 and tabulated in Tables A1 and A2. For both solvent systems, the solubility of N₂O (inverse of Henry's law constant) decreased with increasing temperature and decreased with increasing concentration of the viscosifier.

Further, NaOH in the blend with 38 wt% sugar and 50 wt% glycerol obtained similar Henry's law constant for N₂O at 30 and 40 °C, while at higher temperatures, that of NaOH and sugar was slightly higher.

Kreulen et al. [39] reported the solubility of CO₂ into glycerol/H₂O mixtures at 25 °C, and, similar to this work, the solubility of CO₂ decreased with increasing concentration of glycerol, i.e. increasing solvent viscosity.

4.4. Surface tension and contact angle

To ensure that the addition of the viscosifier to the MEA- and NaOH-based solutions did not change other features of the absorbents, the surface tension of the liquid solutions as well as their contact angle when in contact with the AF2400 layer were characterized. These parameters are important in order to determine the type of contact that can be expected between the liquid phase and the membrane layer.

Table 1
Measured pH at 25 °C for the 30 wt% MEA and 3.9 wt% NaOH solutions with different viscosifier contents.

Solution	pH
30 wt% MEA	12.60
30 wt% MEA + 38 wt% sugar	12.38
3.9 wt% NaOH	13.92
3.9 wt% NaOH + 48 wt% sugar	12.98
3.9 wt% NaOH + 50 wt% glycerol	13.44

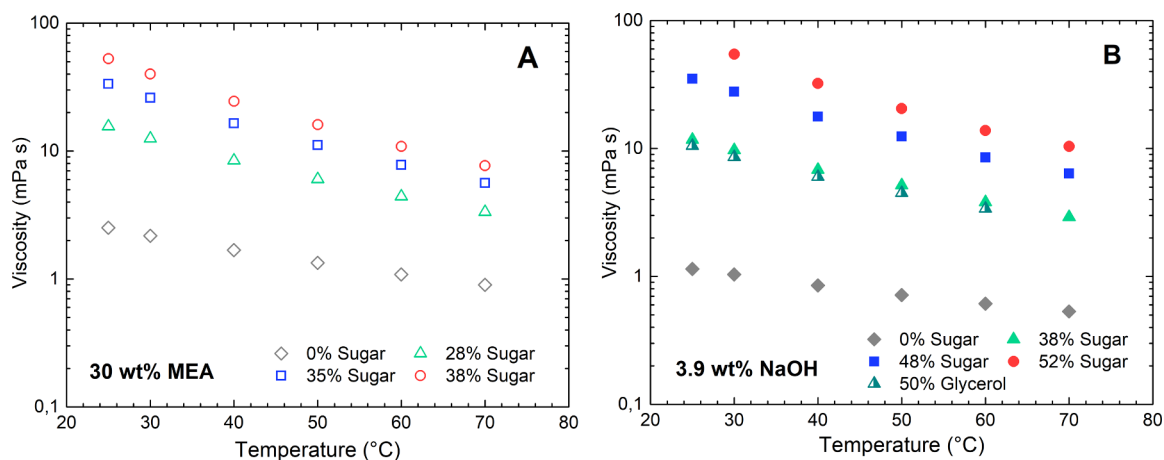


Fig. 7. Viscosity of MEA-based (A) and NaOH-based (B) solutions.

Table 2

Density data for MEA-based solutions, g/cm³.

T (°C)	30 wt% MEA	30 wt% MEA + 28 wt% sugar	30 wt% MEA + 35 wt% sugar	30 wt% MEA + 38 wt% sugar
25	1.012	1.133	1.167	1.185
30	1.009	1.130	1.164	1.182
40	1.005	1.124	1.158	1.176
50	0.999	1.119	1.152	1.170
60	0.994	1.112	1.146	1.163
70	0.988	1.106	1.139	1.157

Fig. 9A shows the results obtained for the surface tension. In the case of 3.9 wt% NaOH, the surface tension was measured to be 70.8 mN/m, which is in line with the literature value [40] and similar to the surface tension reported for water in the same temperature conditions (~72 mN/m at 25 °C, [41]). The low concentration of NaOH is probably related to this latest similarity. The presence of sugar in the NaOH solution did not affect significantly this parameter: deviations lower than 3% were observed up to 52 wt% sugar addition. In the case of 30 wt% MEA, the presence of the amine determined a drop in the surface tension of the liquid solution to 63.5 mN/m, which is determined by the lower surface tension of MEA (48 mN/m, [42]) and in accordance with our previous publication [10] and with literature values [43,44] for a similar amine content. Similar to the NaOH case, the addition of sugar had a minor effect on the surface tension of the more viscous absorbents, with a limited decrease (~5%) at the highest viscosifier contents.

Fig. 9B shows the results obtained in terms of contact angle. Even though in the membrane contactor test the porous layer is not in contact with the liquid (i.e., no wetting can take place), measuring the contact angle can still be important to understand if the viscosifier affects the way that the liquid wets the thin dense coating, possibly affecting the mass transfer. The high content of fluorine within the AF2400 structure makes the polymer highly hydrophobic, resulting in quite high contact angles both in the case of 3.9 wt% NaOH (127°) and

Table 3

Density data for NaOH-based solutions, g/cm³.

T (°C)	3.9 wt% NaOH	3.9 wt% NaOH + 38 wt% sugar	3.9 wt% NaOH + 48 wt% sugar	3.9 wt% NaOH + 52 wt% sugar	3.9 wt% NaOH + 50 wt% glycerol
25	1.040	1.220	1.271	1.307	1.169
30	1.038	1.218	1.269	1.303	1.166
40	1.034	1.213	1.264	1.297	1.161
50	1.030	1.209	1.260	1.291	1.156
60	1.025	1.202	1.253	1.284	1.150
70	1.019	1.196	1.251	1.277	1.143

30 wt% MEA (112°). This last value is in accordance with our previous data [10]. Similar to the surface tension results, the addition of sugar had a limited impact on the contact angle. In the case of NaOH-based absorbents, deviations lower than 1% were observed at increasing liquid viscosity, whereas in the case of MEA-based solutions a minor decrease (~5%) was observed for 28 and 35 wt% sugar.

Overall, it can be concluded quite clearly that the presence of the viscosifier in the absorbents did not affect the wetting behavior with respect to the investigated membranes to a significant extent. Therefore, no influence can be expected from this parameter on the mass transport properties of the absorbents with higher viscosity.

4.5. The overall mass transfer coefficient

4.5.1. String of discs contactor (SDC)

The K_{ov} values obtained from the SDC as a function of temperature are presented in Fig. 10 and tabulated in Tables A3 and A4. For the neat absorbent (0 wt% sugar content), the K_{ov} values for 30 wt% MEA were, as expected, higher than for 3.9 wt% NaOH due to the faster reaction kinetics and the higher solvent concentration of MEA. The K_{ov} further showed dependence on both the temperature and the solvent composition. The K_{ov} increased with increasing temperature, which is likely due to the increasing reaction kinetics and CO₂ diffusivity that follows at higher temperatures, and decreased with the addition of sugar/glycerol to the MEA and NaOH solutions, i.e. decreased with increasing solvent viscosity.

Further, NaOH in the blend with 38 wt% sugar and 50 wt% glycerol, which showed similar solvent viscosity (Section 4.2) and solubility of N₂O (Section 4.3), also obtained similar values for K_{ov} at 30 and 40 °C. At higher temperatures, the K_{ov} values for the NaOH/glycerol solution were slightly higher, which may be related to the difference in N₂O solubility discussed in Section 4.3.

4.5.2. Membrane contactor (MC)

The K_{ov} values obtained from the membrane contactor (MC) at 40 °C are shown in Fig. 11 as a function of the solvent viscosity and tabulated

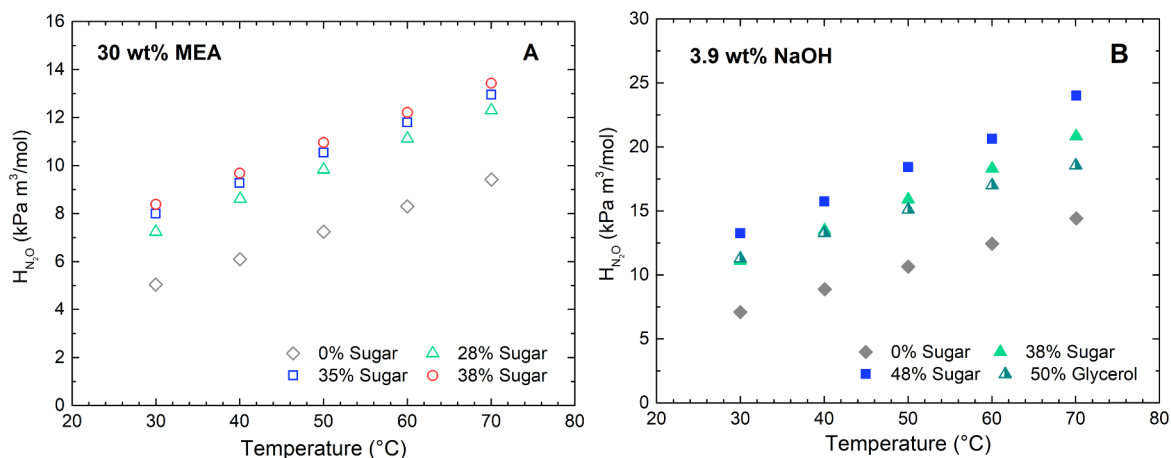


Fig. 8. Henry's law constant for N₂O in (A) MEA-based solutions and (B) NaOH-based solutions.

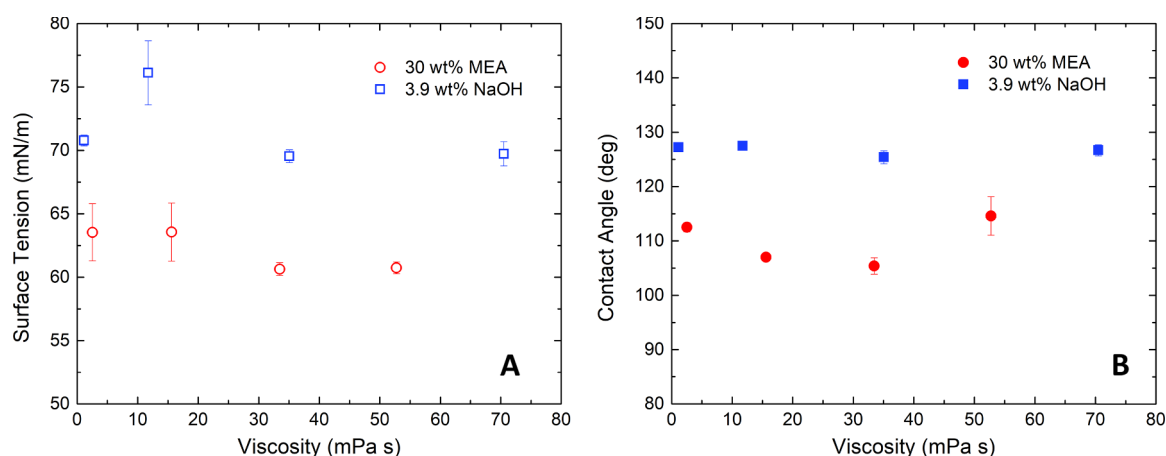


Fig. 9. Surface tension (A) measured for the different MEA- and NaOH-based solutions and contact angle (B) obtained when in contact with an AF2400 coated PP membrane (the viscosity of the 3.9 wt% NaOH + 52 wt% sugar solution was extrapolated).

in Table A5. Like the SDC results presented in Section 4.5.1, the K_{ov} values for 30 wt% MEA were higher than that of 3.9 wt% NaOH, and the K_{ov} values decreased with increasing amount of viscosifier added to the solutions. Also, comparable K_{ov} values were obtained for NaOH in the blend with 38 wt% sugar and 50 wt% glycerol.

Further, from Fig. 11 it can be seen that the K_{ov} values of the MC decreased when p_{CO_2} was increased from 13 kPa to 50 kPa. Based on Eq. (12), the K_{ov} is expected to be independent of the driving force ($\Delta p_{CO_2}^{LM}$)

as also reported by Luo et al. [45]. However, in the MC, the larger CO₂ driving force may have led to a faster increase of the CO₂ loading at the membrane/liquid interface, which would hinder the CO₂ absorption into the liquid phase.

4.5.3. Comparison between the SDC and the MC

When comparing the SDC and the MC results for the neat absorbents, it can be seen that the K_{ov} values of the MC was, as expected,

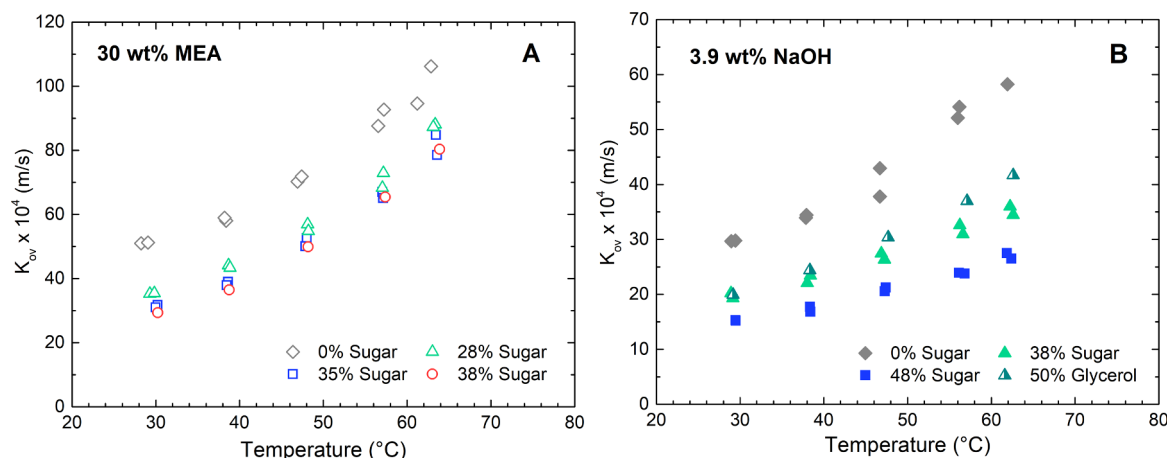


Fig. 10. Calculated values for K_{ov} as a function of temperature obtained from the string of discs contactor for (A) MEA-based solutions and (B) NaOH-based solutions.

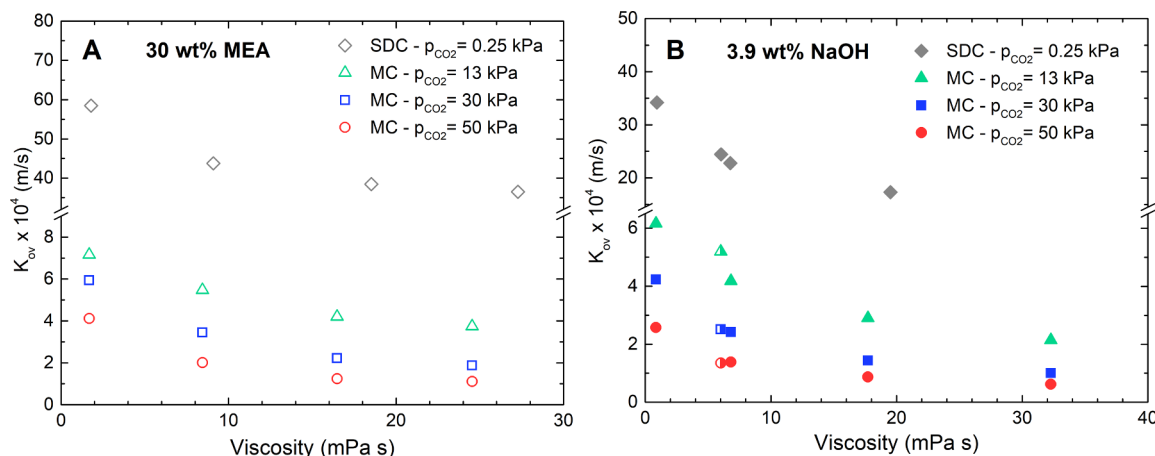


Fig. 11. Calculated values for K_{ov} , as a function of viscosity at 40 °C obtained in the membrane contactor using (A) MEA and (B) NaOH solutions as liquid phases. The semi-empty point in B refer to the results obtained using the solution containing 50 wt% glycerol.

significantly lower than the K_{ov} values calculated from the SDC experiments (Fig. 11). The additional resistance associated with the porous and dense membrane layers is responsible for such a difference. In the case of 30 wt% MEA, the addition of the thin composite membrane appeared to decrease the overall mass transfer coefficient of one order of magnitude. For 3.9 wt% NaOH, the drop was limited to 6 folds. However, a smaller difference in the K_{ov} values might have been obtained if it had been possible to ensure similar driving forces. The MC needs a relatively large CO_2 partial pressure difference between the inlet and outlet of the membrane module to obtain a reliable CO_2 flux, whereas the string of discs contactor can only be operated with low CO_2 driving forces to prevent the amine concentration to be depleted by the reaction.

In addition, unlike the SDC for the neat absorbent, only minor differences in the K_{ov} values from the MC were obtained between 30 wt% MEA ($7.2 \cdot 10^{-4}$ m/s) and 3.9 wt% NaOH ($6.2 \cdot 10^{-4}$ m/s), suggesting that the membrane was contributing to the mass transfer resistance to a larger extent.

Fig. 12 shows the variation of the overall mass transfer coefficient scaled on the value obtained for the solution in the absence of viscosifier ($K_{ov,0}$), as a function of the viscosity increase associated to a given viscosifier content. It appears that the variation observed for the SDC and the MC, when the CO_2 pressure is 13 kPa, lie on the same master curve, independent from the nature of the absorbent. When the content of CO_2 in the feed gas was increased to 30 and 50 kPa, the relative variation decreased for both MEA- and NaOH- based solutions. The results shown in the figure indicate that the performance drop is independent of the solvent system but dependent on the viscosity.

4.6. Modelling

With the aim of improving understanding of the experimental results, the relative contribution of the properties affecting the mass transfer on the liquid side were correlated to the solvent viscosity, and the MC data (at $p_{\text{CO}_2} = 13$ kPa) were compared with the modelled values obtained from Eq. (15). The results obtained at 40 °C are reported in Fig. 13 (MEA) and Fig. 14 (NaOH). First, looking at the relative contributions of the different properties, an increase in solvent viscosity led to two-fold increase of the Henry's law constant for CO_2 (decreasing CO_2 solubility) and fairly constant k_1 values (k_1 - SDC in Figs. 13A and 14A). The k_1 values are further dependent on chemical and physical properties where the liquid viscosity is affecting the flow pattern in the liquid phase and indirectly the diffusion coefficient. However, the decrease in the CO_2 diffusion coefficient, obtained by the modified Stokes-Einstein correlation [46], did not cause a significant decrease in the k_1 values.

The resistance in series model (Eq. (15)) was then applied to predict the K_{ov} values in the MC experiments (Figs. 13B and 14B). Interestingly, although the order of magnitude of the modelled K_{ov} was correct, the model was not able to properly fit the trends observed experimentally. Independently from the absorbent nature, the model approximated nicely the data obtained at low viscosity values, but in the high viscosity range, the modelled mass transfer did not decrease sufficiently to approach the experimental data. In fact, in order to describe the experimental K_{ov} values for the MC, the k_1 (solved from Eq. (15)) should have been reduced two-folds with an increase in solvent viscosity (k_1 - MC in Figs. 13A and 14A). A similar behavior in the modelled K_{ov} was also observed in our previous study [14]. The study suggested that viscous solutions imposed an additional resistance at the membrane/liquid interface leading to a considerably reduction in the CO_2 mass transfer. Along similar lines, Comite et al. [47] suggested a similar conclusion to describe the CO_2 absorption rate into loaded MEA solutions when using a membrane contactor. The study showed that the CO_2 absorption rate decreased with increasing solvent viscosity upon CO_2 loading and an adequate representation of the data was obtained using the liquid film thickness as a fitting parameter in the calculation of the liquid side mass transfer coefficient. The liquid film thickness was modified to account for variations in the solvent viscosity, and a small change in the film thickness could lead to a significant change in the CO_2 flux.

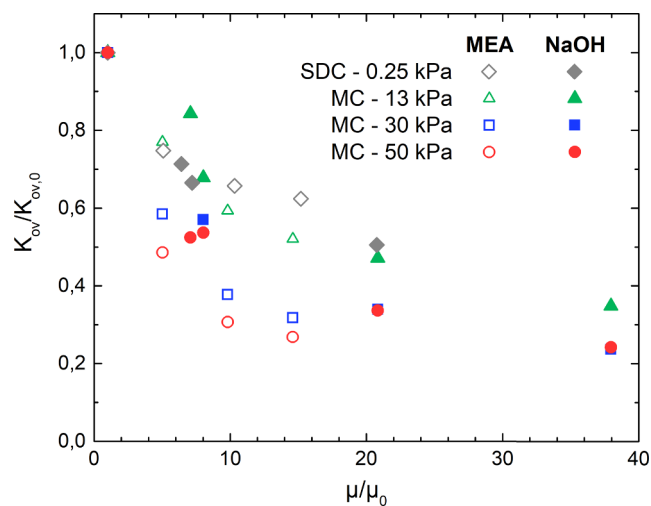


Fig. 12. Variation of the K_{ov} for a given increase of the absorbent viscosity. For both K_{ov} and viscosity (μ), the index “0” refers to the value obtained at 0 wt% content of sugar.

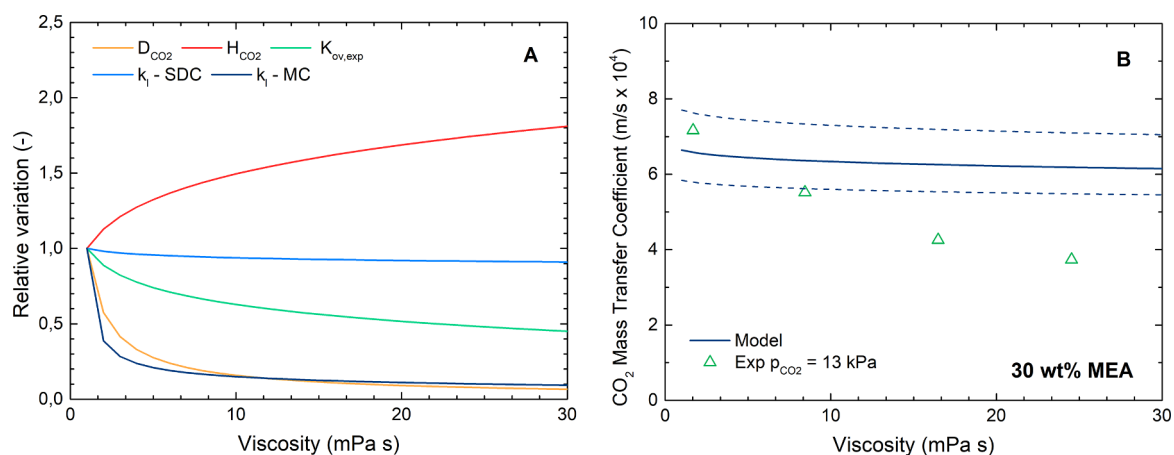


Fig. 13. Modelling of the experimental results for 30 wt% MEA using the resistance in series model for the membrane contactor (Eq. (15)). The dashed lines define the influence of the membrane thickness uncertainty.

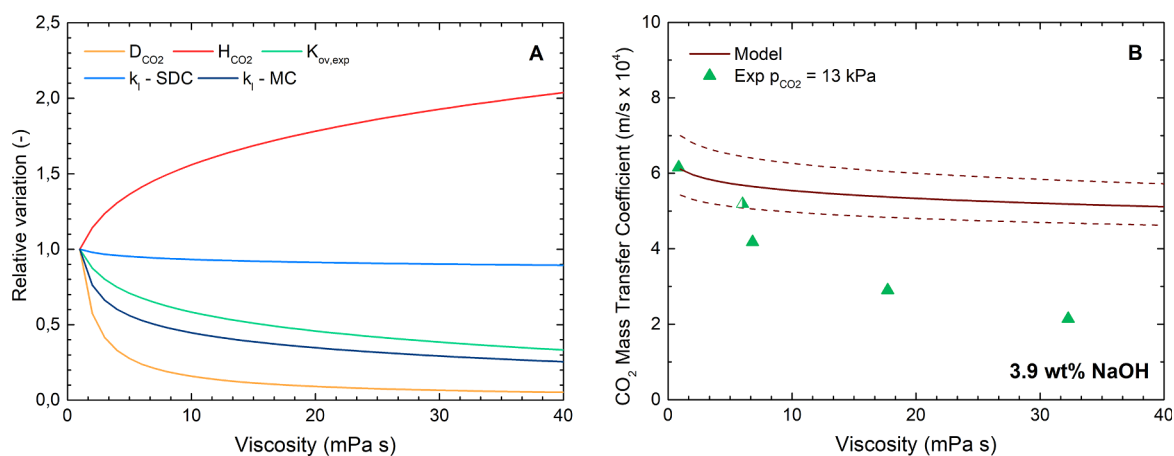


Fig. 14. Modelling of the experimental results for 3.9 wt% NaOH using the resistance in series model for the membrane contactor (Eq. (15)). The dashed lines define the influence of the membrane thickness uncertainty.

Overall, this study indicates that the effect of liquid viscosity on the CO_2 mass transfer in a traditional packed absorption column and a membrane contactor is different. Based on our measurements, the decline in the K_{ov} values obtained from the SDC was due to the decreasing CO_2 solubility and CO_2 diffusion coefficient, while in the MC, the decrease in the K_{ov} values seemed also to be due to other viscosity related effects. Further studies using rigorous thermodynamic and kinetic models to describe the absorption in a membrane contactor are needed to explain the results.

5. Conclusions

This work studied the influence of liquid viscosity on the performance of a thin composite membrane contactor. The viscosity was artificially changed by the addition of sugar and/or glycerol to MEA and NaOH-based solutions, and the overall mass transfer coefficient (K_{ov}) was obtained using a string of discs contactor and a membrane contactor. The K_{ov} was found to decrease with increasing amount of viscosifier, and the decrease seemed to be independent of the solvent system. In the membrane contactor, the K_{ov} decreased as a result of decreasing CO_2 solubility and CO_2 diffusion, and, as the resistance in series model was not able to represent the experimental values, it was

Appendix

See Tables A1-A5.

also likely attributed to an additional resistance established at the membrane/liquid interface.

It is commonly assumed that in membrane contactor applications, the membrane has a dominant role in determining the overall mass transfer resistance, especially when thin composite membranes are used as interface. The present study highlights that a correct solvent selection is also very important to maximize the performance of the membrane contactor for CO_2 capture applications. In particular, the viscosity of the chosen absorbent appears to be a key parameter, dominating over the absorption kinetics. Therefore, even though amine blends have been reported to be a promising development pathway to improve the absorbent performance in traditional packed columns, the increased solvent viscosity can represent a minor limitation for membrane contactor applications. Future work will aim to investigate the reasons of the increased resistance in the membrane contactor system when using viscous solutions.

Acknowledgements

This work was supported by the Research Council of Norway (CLIMIT: New concepts for CO_2 capture, Project No. 239789).

Table A1Henry's law constant for N₂O in MEA-based solutions.

30 wt% MEA		30 wt% MEA + 28 wt% sugar		30 wt% MEA + 35 wt% sugar		30 wt% MEA + 38 wt% sugar	
T (°C)	H _{N₂O} (kPa m ³ /mol)	T (°C)	H _{N₂O} (kPa m ³ /mol)	T (°C)	H _{N₂O} (kPa m ³ /mol)	T (°C)	H _{N₂O} (kPa m ³ /mol)
30.0	5.07	30.0	7.19	30.0	8.04	30.0	8.39
30.0	5.01	30.0	7.29	30.0	7.95	30.0	8.38
40.0	6.10	40.1	8.70	40.0	9.24	40.0	9.71
50.0	7.30	40.1	8.52	40.0	9.30	40.0	9.66
50.0	7.19	50.0	9.96	50.0	10.58	50.0	11.00
60.0	8.27	50.0	9.70	50.0	10.50	50.0	10.93
60.0	8.33	60.0	10.97	60.0	11.76	60.0	12.27
70.0	9.36	60.0	11.27	60.0	11.83	60.0	12.14
70.1	9.48	70.0	12.42	70.0	13.01	70.0	13.36
80.0	10.36	70.0	12.17	70.0	12.88	70.0	13.50
80.0	10.45	80.1	13.28	80.0	13.98	80.0	14.69
90.1	11.65	80.0	13.66	80.0	14.12	80.0	14.50
89.9	11.26	90.0	14.71	90.0	15.24	90.0	15.49
		90.0	14.12	90.0	14.98	90.0	15.69

Table A2Henry's law constant for N₂O in NaOH-based solutions.

3.9 wt% NaOH		3.9 wt% NaOH + 38 wt% sugar		3.9 wt% NaOH + 48 wt% sugar		3.9 wt% NaOH + 50 wt% glycerol	
T (°C)	H _{N₂O} (kPa m ³ /mol)	T (°C)	H _{N₂O} (kPa m ³ /mol)	T (°C)	H _{N₂O} (kPa m ³ /mol)	T (°C)	H _{N₂O} (kPa m ³ /mol)
30.0	7.01	30.0	11.20	30.0	13.11	30.0	11.14
30.0	7.17	30.0	11.04	30.0	13.39	30.0	11.43
40.1	8.78	40.0	13.40	40.1	15.89	40.1	13.52
40.1	9.00	40.0	13.60	40.0	15.60	40.0	13.03
50.0	10.57	50.0	15.90	50.0	18.42	50.0	14.84
50.0	10.72	50.0	15.89	60.0	20.65	50.0	15.37
60.0	12.33	60.0	18.33	60.0	20.60	60.0	17.14
60.0	12.56	60.1	18.28	70.1	24.01	60.1	16.88
70.1	14.42	70.1	20.78	80.0	24.83	70.0	18.47
80.1	16.10	70.1	20.88	80.0	25.50	70.0	18.63
80.1	16.58	80.0	22.57	90.0	27.83	80.0	19.98
90.0	17.96	90.0	23.80	90.0	27.95	80.0	20.12
89.9	17.65	80.0	24.04			90.0	22.86
		90.0	26.98			90.0	22.58

Table A3

Experimental and calculated values for MEA-based solutions using the string of discs contactor (r1 = first run; r2 = second run).

Solution	T (°C)	K _{ov} × 10 ⁴ (m/s)	H _{CO₂} (kPa m ³ /mol)	k _g × 10 ² (m/s)	k _l × 10 ² (m/s)
30 wt% MEA (r1)	28.3	51.0	3.48	3.71	0.82
	38.4	58.0	4.25	3.77	1.12
	46.9	70.2	4.89	3.79	1.58
	56.5	87.6	5.61	3.79	2.33
	61.2	94.6	5.96	3.77	2.71
30 wt% MEA (r2)	29.1	51.2	3.54	3.82	0.83
	38.2	59.0	4.23	3.82	1.14
	47.4	71.9	4.93	3.86	1.63
	57.2	92.7	5.66	3.82	2.53
	62.9	106.2	6.08	3.79	3.21
30 wt% MEA + 28 wt% sugar (r1)	29.3	35.3	5.13	3.85	0.79
	38.7	44.2	6.00	3.87	1.15
	48.1	56.9	6.84	3.92	1.70
	57.2	73.0	7.62	3.90	2.49
	63.4	88.1	8.13	3.84	3.32

(continued on next page)

Table A3 (continued)

Solution	T (°C)	$K_{ov} \times 10^4$ (m/s)	H_{CO_2} (kPa m^3/mol)	$k_g \times 10^2$ (m/s)	$k_l \times 10^2$ (m/s)
30 wt%	29.8	35.5	5.18	3.82	0.80
MEA + 28 wt%	38.9	43.3	6.01	3.83	1.13
sugar (r2)	48.2	54.8	6.85	3.93	1.63
	57.0	68.3	7.60	3.82	2.31
	63.1	87.3	8.11	3.86	3.27
30 wt%	30.2	31.7	5.75	3.80	0.79
MEA + 35 wt%	38.6	39.0	6.50	3.83	1.09
sugar (r1)	48.0	52.6	7.31	3.98	1.66
	57.1	67.0	8.07	3.74	2.40
	63.4	84.8	8.60	3.82	3.35
30 wt%	30.0	31.0	5.73	3.83	0.77
MEA + 35 wt%	38.5	37.9	6.49	3.80	1.05
sugar (r2)	47.9	50.1	7.30	3.84	1.58
	57.1	65.1	8.08	3.84	2.31
	63.6	78.5	8.61	3.77	3.05
30 wt%	30.2	29.4	6.04	3.81	0.76
MEA + 38 wt%	38.8	36.5	6.80	3.87	1.06
sugar	48.2	49.9	7.63	3.96	1.63
	57.4	65.4	8.41	3.89	2.41
	63.9	80.4	8.95	3.87	3.24

Table A4

Experimental and calculated values for NaOH-based solutions using the string of discs contactor (r1 = first run; r2 = second run).

Solution	T (°C)	$K_{ov} \times 10^4$ (m/s)	H_{CO_2} (kPa m^3/mol)	$k_g \times 10^2$ (m/s)	$k_l \times 10^2$ (m/s)
3.9 wt% NaOH (r1)	29.0	29.7	4.93	3.75	0.63
	37.9	33.9	6.06	3.84	0.87
	46.7	37.8	7.17	3.79	1.13
	56.2	54.1	8.37	3.88	1.92
3.9 wt% NaOH (r2)	29.4	29.8	5.00	3.79	0.64
	37.9	34.4	6.07	3.80	0.89
	46.7	42.9	7.17	3.87	1.30
	56.0	52.1	8.35	3.66	1.85
	61.9	58.2	9.10	3.80	2.25
3.9 wt%	29.1	19.3	7.81	3.74	0.63
NaOH + 38 wt%	38.0	22.1	9.30	3.83	0.84
sugar (r1)	47.2	26.3	10.84	3.78	1.15
	56.6	31.0	12.40	3.82	1.52
	62.6	34.5	13.41	3.78	1.82
3.9 wt%	28.9	20.2	7.77	3.75	0.66
NaOH + 38 wt%	38.4	23.4	9.36	3.78	0.90
sugar (r2)	46.9	27.5	10.78	3.79	1.20
	56.2	32.6	12.34	3.81	1.61
	62.2	36.0	13.35	3.78	1.90
3.9 wt%	29.5	15.2	9.60	3.76	0.60
NaOH + 48 wt%	38.4	17.7	11.30	3.83	0.81
sugar (r1)	47.4	21.2	12.98	3.82	1.09
	56.2	23.9	14.65	3.82	1.37
	61.9	27.5	15.41	3.79	1.64
3.9 wt%	29.5	15.3	9.59	3.80	0.61
NaOH + 48 wt%	38.4	16.8	11.29	3.84	0.77
sugar (r2)	47.3	20.5	13.01	3.86	1.06
	56.8	23.8	14.55	3.81	1.34
	62.4	26.5	15.48	3.84	1.58
3.9 wt%	29.1	19.9	8.34	3.73	0.70
NaOH + 50 wt%	38.3	24.4	9.45	3.81	0.95
glycerol	47.7	30.4	10.61	3.88	1.31
	57.1	37.0	11.85	3.85	1.77
	62.6	41.7	12.68	3.74	2.13

Table A5
Experimental values for MEA- and NaOH-based solutions at 40 °C using the membrane contactor.^a

Solution	$K_{ov} \times 10^4$ (m/s)		
	13 vol%	30 vol%	50 vol%
30 wt% MEA	7.2	5.9	4.1
30 wt% MEA + 28 wt% sugar	5.5	3.4	2.0
30 wt% MEA + 35 wt% sugar	4.3	2.2	1.3
30 wt% MEA + 38 wt% sugar	3.7	1.9	1.1
3.9 wt% NaOH	6.2	4.2	2.6
3.9 wt% NaOH + 38 wt% sugar	4.2	2.4	1.4
3.9 wt% NaOH + 48 wt% sugar	2.9	1.4	0.9
3.9 wt% NaOH + 52 wt% sugar	2.1	1.0	0.6
3.9 wt% NaOH + 50 wt% glycerol	5.2	2.5	1.4

^a $k_g = 8.61 \times 10^{-3}$ m/s, $k_m, \delta = 1.8 \mu\text{m} = 7.89 \times 10^{-4}$ m/s.

References

- C. Le Quéré, R.M. Andrew, P. Friedlingstein, S. Sitch, J. Hauck, J. Pongratz, P.A. Pickers, J.I. Korsbakken, G.P. Peters, J.G. Canadell, A. Arneeth, V.K. Arora, L. Barbero, A. Bastos, L. Bopp, F. Chevallier, L.P. Chini, P. Ciais, S.C. Doney, T. Gkritzalis, D.S. Goll, I. Harris, V. Haverd, F.M. Hoffman, M. Hoppema, R.A. Houghton, G. Hurtt, T. Ilyina, A.K. Jain, T. Johannessen, C.D. Jones, E. Kato, R.F. Keeling, K.K. Goldewijk, P. Landschützer, N. Lefèvre, S. Lienert, Z. Liu, D. Lombardozzi, N. Metz, D.R. Munro, J.E.M.S. Nabel, S. Nakaoka, C. Neill, A. Olsen, T. Ono, P. Patra, A. Peregon, W. Peters, P. Peylin, B. Pfeil, D. Pierrot, B. Poulter, G. Rehder, L. Resplandy, E. Robertson, M. Rocher, C. Rödenbeck, U. Schuster, J. Schwinger, R. Séférian, I. Skjelvan, T. Steinhoff, A. Sutton, P.P. Tans, H. Tian, B. Tilbrook, F.N. Tubiello, I.T. van der Laan-Luijckx, G.R. van der Werf, N. Viovy, A.P. Walker, A.J. Wiltshire, R. Wright, S. Zaehle, B. Zheng, *Global Carbon Budget 2018*, *Earth Syst. Sci. Data* 10 (2018) 2141–2194, <https://doi.org/10.5194/essd-10-2141-2018>.
- B. Walsh, P. Ciais, I.A. Janssens, J. Peñuelas, K. Riahi, F. Rydzak, D.P. van Vuuren, M. Obersteiner, Pathways for balancing CO₂ emissions and sinks, *Nat. Commun.* 8 (2017) 14856, <https://doi.org/10.1038/ncomms14856>.
- M. Bui, C.S. Adjiman, A. Bardow, E.J. Anthony, A. Boston, S. Brown, P.S. Fennell, S. Fuss, A. Galindo, L.A. Hackett, J.P. Hallett, H.J. Herzog, G. Jackson, J. Kemper, S. Kreuzer, G.C. Maitland, M. Matuszewski, I.S. Metcalfe, C. Petit, G. Puxty, J. Reimer, D.M. Reiner, E.S. Rubin, S.A. Scott, N. Shah, B. Smit, J.P.M. Trusler, P. Webley, J. Wilcox, N. Mac Dowell, Carbon capture and storage (CCS): the way forward, *Energy Environ. Sci.* 11 (2018) 1062–1176, <https://doi.org/10.1039/C7EE02342A>.
- I.M. Bernhardsen, H.K. Knuutila, A review of potential amine solvents for CO₂ absorption process: absorption capacity, cyclic capacity and pKa, *Int. J. Greenh. Gas Control* 61 (2017) 27–48, <https://doi.org/10.1016/j.ijggc.2017.03.021>.
- S. Liu, H. Gao, C. He, Z. Liang, Experimental evaluation of highly efficient primary and secondary amines with lower energy by a novel method for post-combustion CO₂ capture, *Appl. Energy*. 233–234 (2019) 443–452, <https://doi.org/10.1016/j.apenergy.2018.10.031>.
- A. Sodiq, N. El Hadri, E.L.V. Goetheer, M.R.M. Abu-Zahra, Chemical reaction kinetics measurements for single and blended amines for CO₂ postcombustion capture applications, *Int. J. Chem. Kinet.* 50 (2018) 615–632, <https://doi.org/10.1002/kin.21187>.
- Y. Du, Y. Yuan, G.T. Rochelle, Volatility of amines for CO₂ capture, *Int. J. Greenh. Gas Control* 58 (2017) 1–9, <https://doi.org/10.1016/j.IJGGC.2017.01.001>.
- X. Chen, G. Huang, C. An, Y. Yao, S. Zhao, Emerging N-nitrosamines and N-nitramines from amine-based post-combustion CO₂ capture – a review, *Chem. Eng. J.* 335 (2018) 921–935, <https://doi.org/10.1016/j.cej.2017.11.032>.
- S. Zhao, P.H.M. Feron, L. Deng, E. Favre, E. Chabanon, S. Yan, J. Hou, V. Chen, H. Qi, Status and progress of membrane contactors in post-combustion carbon capture: a state-of-the-art review of new developments, *J. Memb. Sci.* 511 (2016) 180–206, <https://doi.org/10.1016/j.memsci.2016.03.051>.
- L. Ansaloni, A. Arif, A.F. Ciftja, H.K. Knuutila, L. Deng, Development of membrane contactors using phase change solvents for CO₂ capture: material compatibility study, *Ind. Eng. Chem. Res.* 55 (2016) 13102–13113, <https://doi.org/10.1021/acs.iecr.6b03901>.
- L. Ansaloni, R. Rennemo, H.K. Knuutila, L. Deng, Development of membrane contactors using volatile amine-based absorbents for CO₂ capture: amine permeation through the membrane, *J. Memb. Sci.* 537 (2017) 272–282, <https://doi.org/10.1016/J.MEMSCI.2017.05.016>.
- D. deMontigny, P. Tontiwachwuthikul, A. Chakma, Comparing the absorption performance of packed columns and membrane contactors, *Ind. Eng. Chem. Res.* 44 (2005) 5726–5732, <https://doi.org/10.1021/ie040264k>.
- Z. Dai, L. Ansaloni, L. Deng, Precombustion CO₂ capture in polymeric hollow fiber membrane contactors using ionic liquids: porous membrane versus nonporous composite, *Membrane* (2016), <https://doi.org/10.1021/acs.iecr.6b01247>.
- L. Ansaloni, A. Hartono, M. Awais, H.K. Knuutila, L. Deng, CO₂ capture using highly viscous amine blends in non-porous membrane contactors, *Chem. Eng. J.* 359 (2019) 1581–1591, <https://doi.org/10.1016/J.CEJ.2018.11.014>.
- R.J. Mangers, A.B. Ponter, Effect of viscosity on liquid film resistance to mass transfer in a packed column, *Ind. Eng. Chem. Process Des. Dev.* 19 (1980) 530–537, <https://doi.org/10.1021/i260076a005>.
- R. Echarte, H. Campana, E.A. Brignole, Effective areas and liquid film mass transfer coefficients in packed columns, *Ind. Eng. Chem. Process Des. Dev.* 23 (1984) 349–354, <https://doi.org/10.1021/i200025a029>.
- M.M. Delaloye, U. von Stockar, L. Xiao-ping, The influence of viscosity on the liquid-phase mass transfer resistance in packed columns, *Chem. Eng. J.* 47 (1991) 51–61, [https://doi.org/10.1016/0300-9467\(91\)85007-I](https://doi.org/10.1016/0300-9467(91)85007-I).
- D. Song, A.F. Seibert, G.T. Rochelle, Mass transfer parameters for packings: effect of viscosity, *Ind. Eng. Chem. Res.* 57 (2018) 718–729, <https://doi.org/10.1021/acs.iecr.7b04396>.
- E.S. Nakajima, M.C. Maffia, A.J.A. Meirelles, Influence of liquid viscosity and gas superficial velocity on effective mass transfer area in packed columns, *J. Chem. Eng. Jpn.* 33 (2000) 561–566, <https://doi.org/10.1252/jcej.33.561>.
- L. Rizzuti, A. Brucato, Liquid viscosity and flow rate effects on interfacial area in packed columns, *Chem. Eng. J.* 41 (1989) 49–52, [https://doi.org/10.1016/S0300-9467\(98\)80005-1](https://doi.org/10.1016/S0300-9467(98)80005-1).
- D. Song, G.T. Rochelle, Reaction kinetics of carbon dioxide and hydroxide in aqueous glycerol, *Chem. Eng. Sci.* 161 (2017) 151–158, <https://doi.org/10.1016/J.CES.2016.11.048>.
- P.V. Danckwerts, The reaction of CO₂ with ethanolamines, *Chem. Eng. Sci.* 34 (1979) 443–446, [https://doi.org/10.1016/0009-2509\(79\)85087-3](https://doi.org/10.1016/0009-2509(79)85087-3).
- J.E. Crooks, J.P. Donnellan, Kinetics and mechanism of the reaction between carbon dioxide and amines in aqueous solution, *J. Chem. Soc. Perkin Trans. 2* (1989) 331, <https://doi.org/10.1039/p29890000331>.
- A. Fairbourne, G.P. Gibson, D.W. Stephens, The preparation, properties, and uses of glycerol derivatives. Part I. Glycerol ethers, *J. Soc. Chem. Ind.* 49 (1930) 1021–1023, <https://doi.org/10.1002/jctb.5000494903>.
- B.O. Heston, O. Dermer, J.A. Woodside, The reaction of alkoxide ions with carbon dioxide, *Proc. Oklahoma Acad. Sci.* 23 (1943) 67–68.
- A. Hartono, E.O. Mba, H.F. Svendsen, Physical properties of partially CO₂ Loaded Aqueous Monoethanolamine (MEA), *J. Chem. Eng. Data.* 59 (2014) 1808–1816, <https://doi.org/10.1021/je401081e>.
- S. Gondal, N. Asif, H.F. Svendsen, H. Knuutila, Density and N₂O solubility of aqueous hydroxide and carbonate solutions in the temperature range from 25 to 80 °C, *Chem. Eng. Sci.* 122 (2015) 307–320, <https://doi.org/10.1016/j.ces.2014.09.016>.
- D.-Y. Peng, D.B. Robinson, A new two-constant equation of state, *Ind. Eng. Chem. Fundam.* 15 (1976) 59–64, <https://doi.org/10.1021/i160057a011>.
- A. Penttilä, C. Dell'Éra, P. Uusi-Kyyny, V. Alopaeus, The Henry's law constant of N₂O and CO₂ in aqueous binary and ternary amine solutions (MEA, DEA, DIPA, MDEA, and AMP), *Fluid Phase Equilib.* 311 (2011) 59–66, <https://doi.org/10.1016/j.fluid.2011.08.019>.
- S. Ma'mun, V.Y. Dindore, H.F. Svendsen, Kinetics of the reaction of carbon dioxide with aqueous solutions of 2-((2-aminoethyl)amino)ethanol, *Ind. Eng. Chem. Res.* 46 (2007) 385–394, <https://doi.org/10.1021/ie060383v>.
- A. Hartono, E.F. da Silva, H.F. Svendsen, Kinetics of carbon dioxide absorption in aqueous solution of diethylenetriamine (DETA), *Chem. Eng. Sci.* 64 (2009) 3205–3213, <https://doi.org/10.1016/j.ces.2009.04.018>.
- X. Luo, A. Hartono, S. Hussain, H.F. Svendsen, Mass transfer and kinetics of carbon dioxide absorption into loaded aqueous monoethanolamine solutions, *Chem. Eng. Sci.* 123 (2015) 57–69, <https://doi.org/10.1016/j.ces.2014.10.013>.
- S. Gondal, N. Asif, H.F. Svendsen, H. Knuutila, Kinetics of the absorption of carbon dioxide into aqueous hydroxides of lithium, sodium and potassium and blends of hydroxides and carbonates, *Chem. Eng. Sci.* 123 (2015) 487–499, <https://doi.org/10.1016/j.ces.2014.10.038>.
- S. Ma'mun, J.P. Jakobsen, H.F. Svendsen, O. Juliussen, Experimental and modeling study of the solubility of carbon dioxide in aqueous 30 mass % 2-((2-aminoethyl)amino)ethanol solution, *Ind. Eng. Chem. Res.* 45 (2006) 2505–2512, <https://doi.org/10.1021/ie0505209>.
- S.B. Iversen, V.K. Bhatia, K. Dam-Johansen, G. Jonsson, Characterization of microporous membranes for use in membrane contactors, *J. Memb. Sci.* 130 (1997) 205–217, [https://doi.org/10.1016/S0376-7388\(97\)00026-4](https://doi.org/10.1016/S0376-7388(97)00026-4).
- E.N. Fuller, P.D. Schettler, J.C. Giddings, New method for prediction of binary gas-phase diffusion coefficients, *Ind. Eng. Chem.* 58 (1966) 18–27, <https://doi.org/10.1021/ie50677a007>.
- J.K.A. Clarke, Kinetics of absorption of carbon dioxide in monoethanolamine solutions at short contact times, *Ind. Eng. Chem. Fundam.* 3 (1964) 239–245, <https://doi.org/10.1021/i160011a012>.
- J.J. Carroll, J.D. Slupsky, A.E. Mather, The solubility of carbon dioxide in water at

- low pressure, *J. Phys. Chem. Ref. Data* 20 (1991) 1201–1209, <https://doi.org/10.1063/1.555900>.
- [39] H. Kreulen, C.A. Smolders, G.F. Versteeg, W.P.M. van Swaaij, Microporous hollow fibre membrane modules as gas-liquid contactors. Part 1. Physical mass transfer processes: a specific application: mass transfer in highly viscous liquids, *J. Memb. Sci.* 78 (1993) 197–216, [https://doi.org/10.1016/0376-7388\(93\)80001-E](https://doi.org/10.1016/0376-7388(93)80001-E).
- [40] T.F. O'Brien, T.V. Bommaraju, F. Hine, *Handbook of Chlor-Alkali Technology*, Boston, Springer, US, MA, 2005.
- [41] N.B. Vargaftik, B.N. Volkov, L.D. Voljak, International tables of the surface tension of water, *J. Phys. Chem. Ref. Data* 12 (1983) 817–820, <https://doi.org/10.1063/1.555688>.
- [42] Z. Idris, J. Han, S. Jayarathna, D.A. Eimer, Surface tension of alkanolamine solutions: an experimentally based review, *Energy Procedia* 114 (2017) 1828–1833, <https://doi.org/10.1016/j.egypro.2017.03.1310>.
- [43] V.Y. Dindore, D.W.F. Brilman, F.H. Geuzebroek, G.F. Versteeg, Membrane-solvent selection for CO₂ removal using membrane gas-liquid contactors, *Sep. Purif. Technol.* 40 (2004) 133–145, <https://doi.org/10.1016/j.seppur.2004.01.014>.
- [44] P.S. Kumar, J.A. Hogendoorn, P.H.M. Feron, G.F. Versteeg, New absorption liquids for the removal of CO₂ from dilute gas streams using membrane contactors, *Chem. Eng. Sci.* 57 (2002) 1639–1651, [https://doi.org/10.1016/S0009-2509\(02\)00041-6](https://doi.org/10.1016/S0009-2509(02)00041-6).
- [45] X. Luo, A. Hartono, H.F. Svendsen, Comparative kinetics of carbon dioxide absorption in unloaded aqueous monoethanolamine solutions using wetted wall and string of discs columns, *Chem. Eng. Sci.* 82 (2012) 31–43, <https://doi.org/10.1016/j.ces.2012.07.001>.
- [46] G.F. Versteeg, W.P.M. Van Swaaij, Solubility and diffusivity of acid gases (carbon dioxide, nitrous oxide) in aqueous alkanolamine solutions, *J. Chem. Eng. Data* 33 (1988) 29–34, <https://doi.org/10.1021/je00051a011>.
- [47] A. Comite, C. Costa, M. Demartini, R. Di Felice, M. Rotondi, Rate of CO₂ transfer to loaded MEA solutions using a membrane contactor device, *Int. J. Greenh. Gas Control* 52 (2016) 378–386, <https://doi.org/10.1016/J.IJGGC.2016.07.029>.